Microtubule-directed transport of purine metabolons drives their cytosolic transit to mitochondria

Chung Yu Chan[a,b,1], Anthony M. Pedley[b,1], Doory Kim[c,1,2], Chenglong Xia[c], Xiaowei Zhuang[c,d,e,3], and Stephen J. Benkovic[b,3]

[a]Department of Engineering Science and Mechanics, The Pennsylvania State University, University Park, PA 16802; [b]Department of Chemistry, The Pennsylvania State University, University Park, PA 16802; [c]Department of Chemistry and Chemical Biology, Harvard University, Cambridge, MA 02138; [d]Howard Hughes Medical Institute, Harvard University, Cambridge, MA 02138; and [e]Department of Physics, Harvard University, Cambridge, MA 02138

Edited by David G. Drubin, University of California, Berkeley, California, and accepted by Editorial Board Member Michael R. Botchan November 4, 2018 (received for review August 14, 2018)

To meet their purine demand, cells activate the de novo purine biosynthetic pathway and transiently cluster the pathway enzymes into metabolons called purinosomes. Recently, we have shown that purinosomes were spatially colocalized with mitochondria and microtubules, yet it remained unclear as to what drives these associations and whether a relationship between them exist. Here, we employed superresolution imaging methods to describe purinosome transit in the context of subcellular localization. Time-resolved imaging of purinosomes showed that these assemblies exhibit directed motion as they move along a microtubule toward mitochondria, where upon colocalization, a change in purinosome motion was observed. A majority of purinosomes colocalized with mitochondria were also deemed colocalized with microtubules. Nocodazole-dependent microtubule depolymerization resulted in a loss in the purinosome–mitochondria colocalization, suggesting that the association of purinosomes with mitochondria is facilitated by microtubule-directed transport, and thereby supporting our notion of an interdependency between these subcellular components in maximizing purine production through the de novo purine biosynthetic pathway.

purine metabolism | metabolon | superresolution microscopy | mitochondria | cytoskeleton

An emerging trend in metabolism is that metabolic enzymes form supramolecular complexes, called metabolons, to enhance metabolic flux (1–4). Unlike previously reported metabolons in the tricarboxylic acid cycle (5) and glycolysis (6), enzymes within the de novo purine biosynthetic pathway assemble into transient, nonmembrane-bound clusters called purinosomes (2, 7, 8). Proximity assays demonstrated that purinosomes are composed of core and peripheral proteins and likely assemble in a step-wise manner (9, 10). Further characterization of purinosome regulation revealed that formation is likely mediated through the involvement of molecular chaperones (11, 12) and kinases (13, 14). The degree of purinosome assembly is reflected in the cell's overall intracellular purine demand and serves as a biomarker for pathway activation (15). Under cellular conditions that promote purinosome formation, the metabolic flux through the pathway was shown to be enhanced (16).

Recently, imaging studies had revealed colocalization between purinosomes and subcellular structures (i.e., mitochondria and microtubules) in HeLa cells, suggesting that the purinosome might be highly dependent on one or the other for spatial organization within the cell (14, 17). The de novo process in which the purines are made is energy-intensive and requires five molecules of ATP, numerous substrates, and cofactors for every molecule of inosine monophosphate generated. Studies have shown that the formate exported from mitochondria is an essential precursor for the 10-formyltetrahydrofolate cofactor, and elevated production of mitochondrial formate results in enhanced metabolic flux through the pathway (18). These observations help support the hypothesis that close proximity of purinosomes to mitochondria would be advantageous in meeting the catalytic demands of the enzymes.

In this study, we employed a combination of stochastic optical reconstruction microscopy (STORM) (19) and instantaneous structured illumination microscopy (VT-iSIM) to visualize the localization and movement of purinosomes within the cytosol of hypoxanthine-guanine phosphoribosyltransferase (HPRT)-deficient fibroblasts derived from patients diagnosed with Lesch-Nyhan disease (20). These cells rely on the de novo purine biosynthetic pathway to generate purines and show a twofold enrichment of purinosome-positive cells compared with a normal, asynchronous fibroblast cell population (20). By using STORM, the average diameter and density distributions of purinosomes in Lesch-Nyhan disease are shown to be comparable with those in purine-depleted HeLa cells (*SI Appendix*, Fig. S1). Colocalization analysis of FGAMS, our marker for the purinosome, with either mitochondria or microtubules was performed by 3D STORM (21) and resulted in a high degree of colocalization, similar to that of our previous studies in purine-depleted HeLa cells (14). Depending on their colocalization mitochondria or microtubules, different types of motions were revealed for purinosomes through time-lapse imaging by VT-iSIM. Characterization of directed motions revealed a high tendency for purinosomes to be localized to microtubules and their motion directed toward mitochondria, suggesting a mechanism by which purinosomes are trafficked to mitochondria via the microtubule network. Disruption of this network resulted in a decrease in purinosome–mitochondria colocalization,

Significance

This study draws on the power of superresolution microscopy to investigate how metabolons behave near different subcellular components. We revealed an interdependent relationship among purinosomes, mitochondria, and microtubules. This further suggests a role for each in maximizing purine production in times of high intracellular demand. With the increasing number of reported metabolons, this study has uncovered a potential general strategy for how metabolons use subcellular networks to facilitate metabolic trade between themselves and other cellular organelles.

Author contributions: C.Y.C., X.Z., and S.J.B. designed research; C.Y.C., A.M.P., D.K., and C.X. performed research; C.Y.C., A.M.P., D.K., and C.X. analyzed data; and C.Y.C., A.M.P., X.Z., and S.J.B. wrote the paper.

The authors declare no conflict of interest.

This article is a PNAS Direct Submission. D.G.D. is a guest editor invited by the Editorial Board.

[1]C.Y.C., A.M.P., and D.K. contributed equally to this work.

[2]Present address: Department of Chemistry, Hanyang University, Seoul, South Korea 133-791.

[3]To whom correspondence may be addressed. Email: zhuang@chemistry.harvard.edu or sjb1@psu.edu.

This article contains supporting information online at www.pnas.org/lookup/suppl/doi:10.1073/pnas.1814042115/-/DCSupplemental.

Published online December 3, 2018.

supporting the notion of an interplay between these subcellular bodies.

Results

Colocalization of Purinosomes with Mitochondria and Microtubules by Two-Color STORM. Colocalization studies of purinosomes with mitochondria in HPRT-deficient fibroblasts were performed using two-color 3D STORM imaging of cells transiently expressing the purinosome marker FGAMS-mMaple3 and immunostaining the mitochondrial outer membrane translocase (TOM20) with the photoswitchable dye Alexa Fluor 647 (Fig. 1 *A* and *B*). The percentage of purinosomes colocalized with mitochondria was found to be 81.4 ± 6.7%, which was significantly higher than that obtained from the randomized distribution of purinosomes in the cytosol (42.9 ± 6.3%; $P < 0.05$; Fig. 1*C* and *SI Appendix*, *Supplementary Materials and Methods*).

We also observed a high level of colocalization between purinosomes (FGAMS-mMaple3) and microtubules immunolabeled with Alexa Fluor 647 (Fig. 1 *D* and *E*). Statistical analysis showed that the purinosome–microtubules colocalization percentage was 91.6 ± 3.0%, which was significantly higher than that of a randomized purinosome distribution (60.5 ± 5.6%; $P < 0.05$; Fig. 1*F*). Given the high percentages of purinosomes that are colocalized with mitochondria (81.4%) and microtubules (91.6%), it is likely that a significant number of the purinosomes are simultaneously colocalized with both mitochondria and microtubules.

Colocalization of Purinosomes with Mitochondria and Microtubules by Three-Color VT-iSIM. To obtain further evidence that some purinosomes are colocalized with both mitochondria and microtubules, we performed three-color imaging of live cells, using VT-iSIM (Fig. 2*A*). The general localization of purinosomes with mitochondria and microtubules is illustrated in the representative region of interest (ROI; Fig. 2*A*, *Inset*). The image in the ROI is split into individual channels for better visualization (Fig. 2*B*). We found 57.1 ± 13.2% of purinosomes colocalized with mitochondria, which is statistically greater than the randomization control (22.5 ± 10.2%; $P < 0.05$; Fig. 2*C*). Substantial purinosome–mitochondria colocalization was thus observed with both imaging methods, and the quantitative difference in the extent of colocalization observed between the two methods may be attributed to differences in the acquisition and image analysis methods, or sample-to-sample variations. Furthermore, we observed that essentially all mitochondria-associated purinosomes were also colocalized with microtubules (Fig. 2*D*). Of the remaining purinosomes, the majority (86%) were also associated with microtubules. These observations invite the question as to whether microtubules drive purinosome–mitochondria colocalization.

Analysis of Purinosome Motions with Respect to Mitochondria and Microtubules. To evaluate purinosome motions in live cells with respect to both mitochondria and microtubules, three-color time-lapse images were captured, revealing the interplay between these three subcellular components during a 495-s (5 s/frame, 100 frames) time

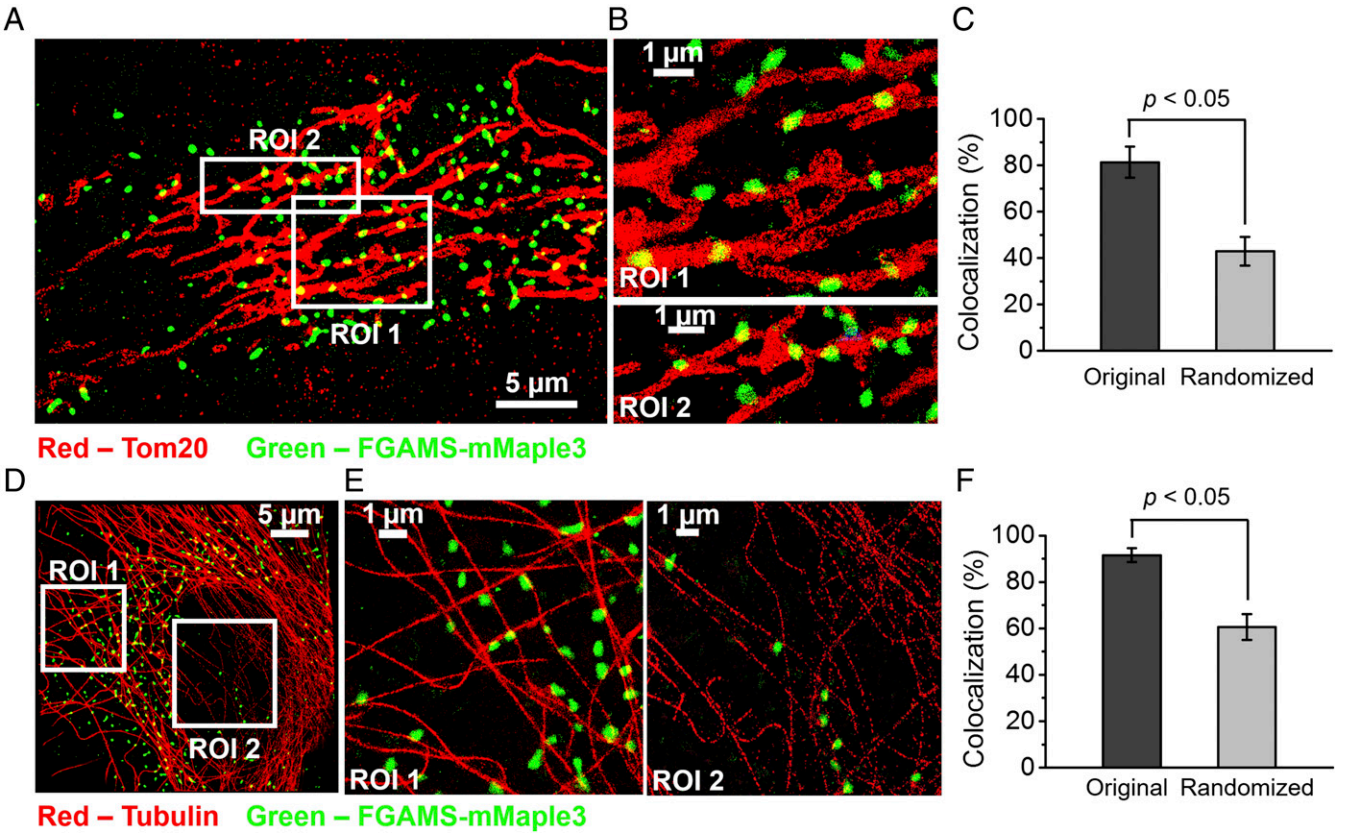

Fig. 1. STORM imaging of purinosomes with mitochondria or microtubules in HPRT-deficient fibroblasts. (*A*) 2D projection of 3D STORM image showing the proximity of purinosome marker protein, FGAMS-mMaple3 (green), to TOM20 (red), an outer mitochondrial membrane protein, in an HPRT-deficient fibroblast. (*B*) Magnified ROIs from *A*. (*C*) Colocalization between purinosomes and mitochondria was found to be 81.3 ± 6.7%, and was shown to be significantly higher than that of a randomized purinosome distribution (42.9 ± 6.3%). Data are presented as mean ± SD, $n = 14$ cells, $P < 0.05$, as calculated by paired t test. (*D*) 2D projection of 3D STORM image showing the proximity of FGAMS-mMaple3 (green) with tubulin (red) in an HPRT-deficient fibroblast. (*E*) Magnified ROIs from *D*. (*F*) Statistical analysis of the colocalization between purinosomes and microtubules was calculated to be 91.6 ± 3.0%, and was significantly higher than that of a randomized purinosome distribution (60.6 ± 5.6%). Data are presented as mean ± SD, $n = 14$ cells, $P < 0.05$, as calculated by paired t test.

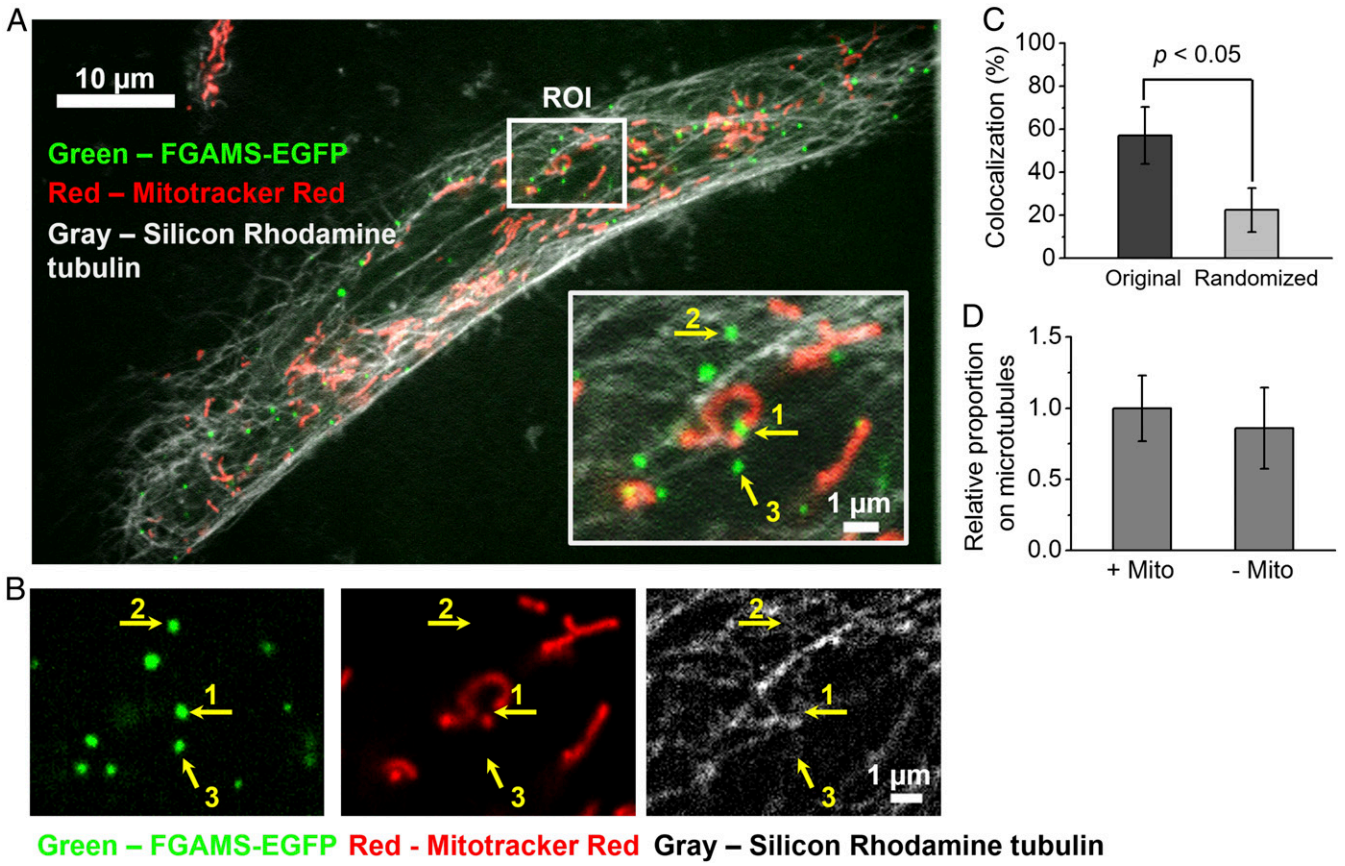

Fig. 2. Colocalization of purinosomes with mitochondria and microtubules, using high-resolution confocal microscopy. (*A*) Representative three-color image by VT-iSIM showing purinosomes (FGAMS-EGFP, green) that were localized in the network of mitochondria (MitoTracker Red, red) and microtubules (silicon-rhodamine tubulin, gray) in HPRT-deficient fibroblasts at a given time. (*Inset*) Magnified ROIs from *A* illustrating different type of purinosome colocalizations with respect to a subcellular structure of interest (1, mitochondrion; 2, microtubule; and 3, neither mitochondrion nor microtubule). (*B*) The individual channels for purinosomes, mitochondria, and microtubules of the ROI in *A*. (*C*) Average colocalization percentage between purinosomes and mitochondria in HPRT-deficient fibroblasts. (*D*) Further classification of the mitochondria-colocalized purinosomes (+Mito) and nonmitochondria-colocalized purinosomes (–Mito). The relative proportion of the +Mito group that were also colocalized with microtubules was 1.00 ± 0.23, indicating that large proportion of purinosomes (57.1 ± 13.2% of total purinosomes) were dual-colocalized with both mitochondria and microtubules. For the –Mito group, 86.0 ± 29% of them (36.9 ± 12.3% of total) were colocalized with microtubule.

course (Movie S1). During this time, the number of purinosomes in a given cell did not drastically change ($n = 30$ cells, 3,784 purinosomes) (*SI Appendix*, Fig. S2). The motions of purinosomes depended strongly on their colocalization with other subcellular structures. Mean squared displacement (MSD) analyses of purinosome trajectories in the *x-y* plane revealed three types of motion: normal diffusion, constrained motion, and directed motion.

The majority of purinosomes that were colocalized with both mitochondria and microtubules (84%) showed constrained (nondirected) motion (see Fig. 4*A*). As illustrated in Fig. 3*A*, a purinosome (yellow arrow) displayed minimal displacement while colocalized with both mitochondria and microtubules (Fig. 3*B* and Movie S2). The MSD of this trajectory (solid black line) demonstrated constrained motion, as characterized by an asymptotic behavior of MSD over Δt (red dashed line, Fig. 3*C*). The remaining dual-colocalized purinosomes (16%) showed a limited directed motion that is attributed to its travel along a microtubule as it approaches a mitochondrion. The motions of such a purinosome (yellow arrow) moving along a microtubule from point A to B are shown in Fig. 3*D* (Movie S3). Here, the purinosome showed directed motion as it moved toward a mitochondrion along a microtubule from 0 to 140 s (Fig. 3 *E* and *F*, *Upper*). Once colocalized with the mitochondrion, the purinosome showed constrained motion (Δt = 145–245 s; Fig. 3*F*, *Lower*). The purinosomes that were not colocalized with either mitochondria or microtubules showed relatively small displacement (Fig. 3 *G* and *H* and Movie S4). These purinosomes showed a linear dependence of MSD on Δt (Fig. 3*I*, red dashed line), as shown by the representative purinosome in Fig. 3*G*. The median value of the diffusion coefficient of purinosomes was calculated to be 4.5×10^{-4} μm^2/s ($n = 25$).

We next asked how general such purinosome behaviors are across a number of cells (Fig. 4*A*). Within the 30 cells, 135 purinosomes were analyzed over the course of 4,135 total time frames. The distance a purinosome traveled between two consecutive frames for both directed and nondirected motions was calculated (Fig. 4*B*). For directed motions, the median value from the distribution of distances was 344 nm and is distinct from the population of purinosomes displaying nondirectional motions (Fig. 4*B*). The calculated mean velocity for these purinosomes during directed motion was determined by MSD fitting to be 55.2 nm/s (*SI Appendix*, Fig. S3), with a median time for the duration of directed motion of 20 s (Fig. 4*C*; $n = 100$ representative trajectories).

Validation of Microtubule-Assisted Directed Motion of Purinosomes Was Observed on Disruption of Microtubule Polymerization with Nocodazole. Microtubule depolymerization was first detected after 30 min of treatment with nocodazole, and within 2 h, complete depolymerization

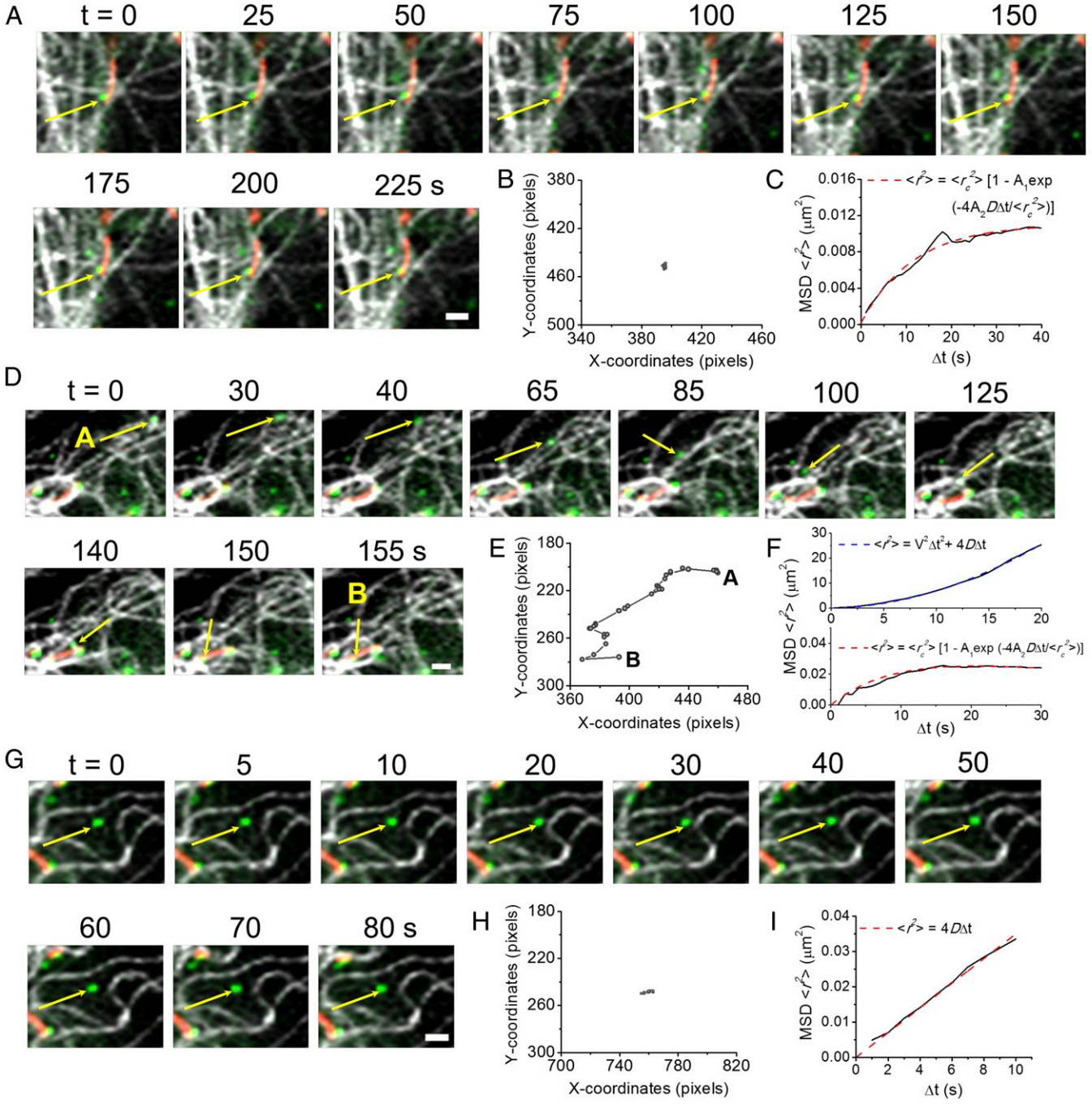

Fig. 3. Characterization of purinosomes based on both their localization and MSD analyses in HPRT-deficient fibroblasts. (*A*) Representative time-lapse three-color images showing a purinosome (FGAMS-EGFP, green) colocalized with both mitochondria (MitoTracker Red, red) and microtubules (silicon-rhodamine tubulin, gray; yellow arrow). Portion of a purinosome colocalized with mitochondria is shown as yellow. (*B*) Trajectory of the specified purinosome from *A* in *x-y* coordinates. The purinosome was colocalized with mitochondria and demonstrated very minimal displacement over the course of 225 s. (*C*) Time-average MSD plot of the trajectory in *B* (solid black line) fitted with the equation for constrained motion (dashed red line). (*D*) Representative time-lapse three-color images showing a purinosome (yellow arrow) colocalized with only microtubules initially. From 0 to 140 s, the purinosome moved along a microtubule and then became colocalized with a mitochondrion from 140 to 155 s. (*E*) Trajectory of the specified purinosome from *D* in *x-y* coordinates that demonstrated a much larger displacement than the purinosome in *A*. (*F*) Time-average MSD plot of the trajectory in *E* (solid black line) revealed a biphasic behavior. The MSD of this trajectory was first fitted with the quadratic equation for directed motion (*Upper*, dashed blue line, 0–140 s) and then constrained motion as in *C* (*Lower*, dashed red line, 140–155 s). (*G*) Representative time-lapse three-color images showing a purinosome (yellow arrow) not colocalized with either mitochondria or microtubules. (*H*) Trajectory of the specified purinosome from *G* in *x-y* coordinates. This purinosome displayed random motion with minimal displacement. (*I*) Time-average MSD plot of the trajectory in *H* (solid black line) fitted with the equation for normal diffusion (dashed red line).

was noted (*SI Appendix*, Fig. S4). We next imaged purinosome-positive cells that were costained for mitochondria to ask whether purinosome–mitochondria colocalization in cells changed as a function of time after nocodazole treatment. A representative cell showing the lack of colocalization between purinosomes (green) and mitochondria (red) after 2 h of nocodazole treatment

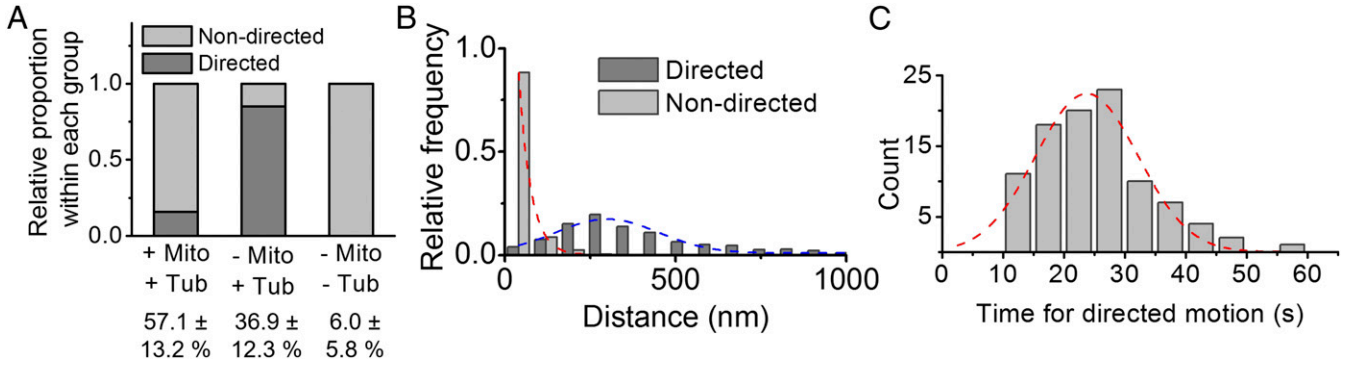

Fig. 4. Statistical analyses of purinosome motions based on both their localization and MSD in HPRT-deficient fibroblasts. (*A*) Relative proportion of trajectories that displayed directed motion. Of those purinosomes colocalized with microtubules but not mitochondria (−Mito, +Tub), 85% had directed motion, whereas 16% of dual-colocalized purinosomes (+Mito, +Tub) had directed motion. Those purinosomes not colocalized with either (−Mito, −Tub), and did not have any directed motion. $n = 50$ representative trajectories for dual-colocalized and microtubule-colocalized purinosomes; $n = 28$ representative trajectories for nonlocalized purinosomes. The percentage of purinosomes in their respective group [(±) mito or tub] is also shown. (*B*) Distribution of the distance a purinosome traveled between two consecutive frames in a trajectory. For those that were on the microtubule only, the median distance that a purinosome traveled between two consecutive frames in a directed motion was 344 nm. $n = 30$ cells, 135 purinosomes, 4,135 total frames. (*C*) A frequency plot of the time that a purinosome displayed directed motion. The median value is 20 s. Data are presented as accumulated count, $n = 100$ representative trajectories.

is shown in Fig. 5 *A* and *B*. Unlike HeLa cells, no significant change in the number of purinosomes per HPRT-deficient fibroblast was observed postnocodazole treatment (17). The degree of purinosome–mitochondria colocalization postnocodazole treatment decreased substantially (from 57.1 ± 13.2% to 23.8 ± 2.1%) after 3 h of treatment, with a randomized control of 12.9 ± 3.7% (Fig. 5*C* and *SI Appendix*, Fig. S5). Purinosomes not colocalized with mitochondria postnocodazole treatment displayed normal diffusion, with a median diffusion coefficient of 1.8×10^{-4} μm^2/s ($n = 34$) during the 495-s time course (Fig. 5 *B* and *D*, *SI Appendix*, Fig. S6, and Movie S5). These results suggest that microtubule-directed movement of purinosome is important for purinosome–mitochondria colocalization.

The collective analysis of purinosomes (n = 50/time point) showed a time-dependent reduction in directed motion when the duration of nocodazole treatment increased (Fig. 5*E* and *SI Appendix*, Fig. S7). After 3 h of treatment, the proportion of directed motion in purinosomes, not colocalized with mitochondria,

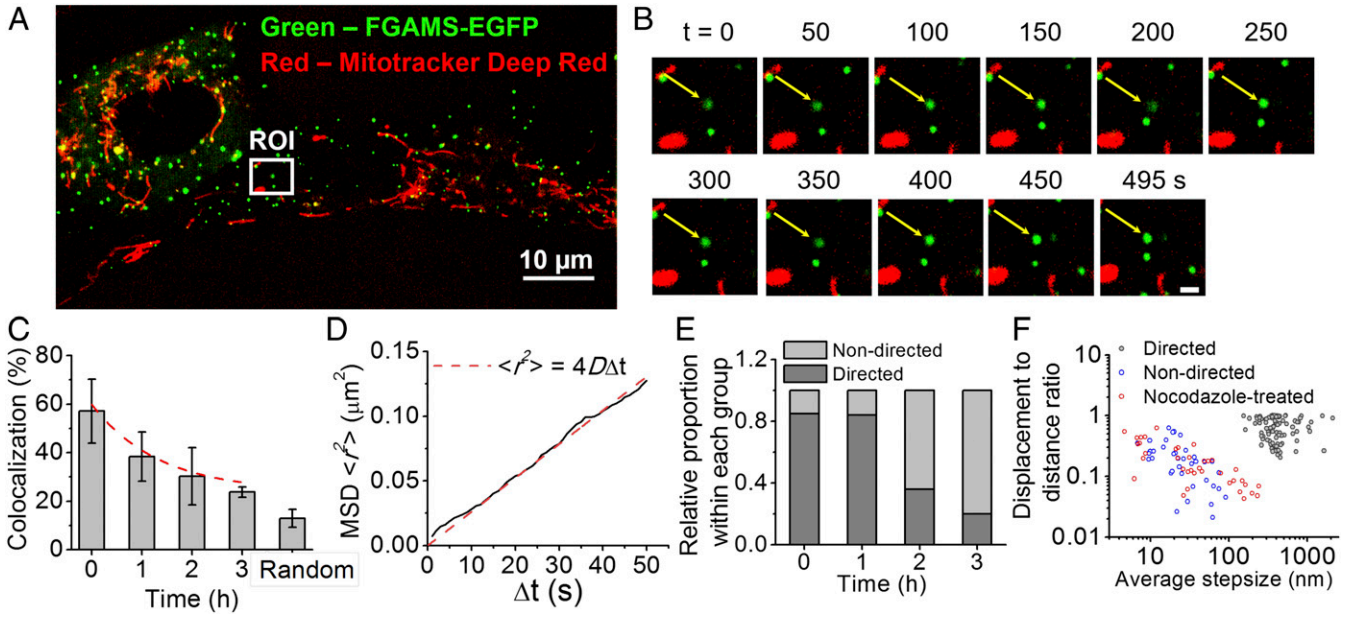

Fig. 5. Effect of nocodazole treatment on purinosomes localization and motion in HPRT-deficient fibroblasts. (*A*) Representative two-color image showing the relative position of purinosomes (FGAMS-EGFP, green) to mitochondria (MitoTracker Deep Red, red) 2 h postnocodazole treatment. (*B*) Time-lapse images of the magnified ROI from *A* showing a purinosome (white arrow) that did not become colocalized with mitochondria during the study. (Scale bar, 1 μm.) (*C*) Purinosome–mitochondria colocalization percentage as a function of time postnocodazole treatment. Data are presented as mean ± SD, $n = 30$ cells from four independent experiments. (*D*) Time-average MSD plot of the trajectory in *B* (solid black line) fitted with the equation for normal diffusion (dashed red line). The diffusion coefficient of this purinosome was estimated as 6.55×10^{-4} μm^2/s from data fitting. (*E*) Relative proportion of trajectories that displayed directed or nondirected motions as a function of time postnocodazole treatment. Only the trajectories of purinosomes not colocalized with mitochondria (−mito) were analyzed. $n = 50$ representative trajectories for each point. (*F*) A scatterplot of the displacement-to-distance ratio (DDR) vs. average step-size for each trajectory at t = 0 (control) and t = 2 h postnocodazole treatment (red). $n = 183$ total representative trajectories. The control trajectories were further partitioned into two categories: directed (black) and nondirected (blue).

decreased from greater than 85% to less than 20%. Finally, we compared the displacement-to-distance ratio and the average step size of the purinosome trajectories in untreated condition and at 2 h postnocodazole treatment (Fig. 5*F*). Displacement-to-distance ratio is defined as the ratio a purinosome is displaced between the initial and final positions over the sum of the distances between consecutive positions during the time course. The nocodazole-treated trajectories distinctly clustered with those purinosomes having nondirected motions in the untreated control, further supporting the notion that the directed motion of purinosomes is attributed to its colocalization with microtubules.

Discussion

This study examined the spatiotemporal relationship among purinosomes, mitochondria, and microtubules. Of the purinosomes colocalized with microtubules, but not simultaneously with mitochondria, the vast majority showed directed motion along microtubules with a mean velocity of 55 nm/s. A wide range of transport velocities on microtubules have been observed, from several tens of nanometers per second >1 μm/s (22–24), and the velocity that we observed here for purinosome is similar to the directed movement of RNA granules along dendrites in neurons (ca. 50 nm/s) (25). Disruption of the microtubule polymerization by nocodazole led to a decrease in purinosome–mitochondria colocalization and a loss of directed motion. Results with the nocodazole treated cells support the importance of the microtubules both for purinosome movement and for the association of purinosome with mitochondria.

The de novo purine synthesis pathway enzymes require cofactors such as ATP and folate, both of which are products of mitochondrial metabolism. In contrast, the ultimate products of a purinosome are AMP and GMP, and GMP is essential for mitochondrial DNA synthesis. Therefore, the formation of the purinosome metabolon cannot only facilitate flux from phosphoribosyl pyrophosphate to AMP/GMP by the encapsulation of constituent enzymes but can also, through its association with mitochondrion, act as an import/export agent for metabolites responsible for the function of both. We speculate that in general, metabolic pathways could be likewise organized into metabolons that are actively transported to distinct complementary cellular organelles to maximize both their functions.

Materials and Methods

Materials and experimental procedures for plasmids and antibodies, cell culture and transient transfection of mammalian cells, STORM, high-resolution confocal microscopy, immunostaining for STORM, STORM colocalization analysis, high-resolution confocal colocalization analysis, randomized colocalization analysis, image visualization and statistical trajectory analysis of the representative three-color images, fitting of the time-averaged MSD, and nocodazole treatment experiment are described in the *SI Appendix, Supplementary Materials and Methods*.

ACKNOWLEDGMENTS. We thank Dr. H. A. Jinnah at Emory University for providing us with the HPRT-deficient fibroblasts used in this study and Dr. J. R. Pritchard and S. Leighow at The Pennsylvania State University for the assistance in MatLab coding. This work was funded by National Institutes of Health Grant GM024129 (to S.J.B.) and The Howard Hughes Medical Institute (X.Z.).

1. Srere PA (1985) The metabolon. *Trends Biochem Sci* 10:109–110.
2. Pedley AM, Benkovic SJ (2017) A new view into the regulation of purine metabolism: The purinosome. *Trends Biochem Sci* 42:141–154.
3. Wilson MZ, Gitai Z (2013) Beyond the cytoskeleton: Mesoscale assemblies and their function in spatial organization. *Curr Opin Microbiol* 16:177–183.
4. Castellana M, et al. (2014) Enzyme clustering accelerates processing of intermediates through metabolic channeling. *Nat Biotechnol* 32:1011–1018.
5. Barnes SJ, Weitzman PDJ (1986) Organization of citric acid cycle enzymes into a multienzyme cluster. *FEBS Lett* 201:267–270.
6. Campanella ME, Chu H, Low PS (2005) Assembly and regulation of a glycolytic enzyme complex on the human erythrocyte membrane. *Proc Natl Acad Sci USA* 102:2402–2407.
7. Zhao H, French JB, Fang Y, Benkovic SJ (2013) The purinosome, a multi-protein complex involved in the de novo biosynthesis of purines in humans. *Chem Commun (Camb)* 49:4444–4452.
8. An S, Kumar R, Sheets ED, Benkovic SJ (2008) Reversible compartmentalization of de novo purine biosynthetic complexes in living cells. *Science* 320:103–106.
9. Deng Y, et al. (2012) Mapping protein-protein proximity in the purinosome. *J Biol Chem* 287:36201–36207.
10. Kyoung M, Russell SJ, Kohnhorst CL, Esemoto NN, An S (2015) Dynamic architecture of the purinosome involved in human de novo purine biosynthesis. *Biochemistry* 54: 870–880.
11. French JB, et al. (2013) Hsp70/Hsp90 chaperone machinery is involved in the assembly of the purinosome. *Proc Natl Acad Sci USA* 110:2528–2533.
12. Pedley AM, Karras GI, Zhang X, Lindquist S, Benkovic SJ (2018) Role of HSP90 in the regulation of de novo purine biosynthesis. *Biochemistry* 57:3217–3221.
13. An S, Kyoung M, Allen JJ, Shokat KM, Benkovic SJ (2010) Dynamic regulation of a metabolic multi-enzyme complex by protein kinase CK2. *J Biol Chem* 285:11093–11099.
14. French JB, et al. (2016) Spatial colocalization and functional link of purinosomes with mitochondria. *Science* 351:733–737.
15. Chan CY, et al. (2015) Purinosome formation as a function of the cell cycle. *Proc Natl Acad Sci USA* 112:1368–1373.
16. Zhao H, et al. (2015) Quantitative analysis of purine nucleotides indicates that purinosomes increase de novo purine biosynthesis. *J Biol Chem* 290:6705–6713.
17. An S, Deng Y, Tomsho JW, Kyoung M, Benkovic SJ (2010) Microtubule-assisted mechanism for functional metabolic macromolecular complex formation. *Proc Natl Acad Sci USA* 107:12872–12876.
18. Tibbetts AS, Appling DR (2010) Compartmentalization of mammalian folate-mediated one-carbon metabolism. *Annu Rev Nutr* 30:57–81.
19. Rust MJ, Bates M, Zhuang X (2006) Sub-diffraction-limit imaging by stochastic optical reconstruction microscopy (STORM). *Nat Methods* 3:793–795.
20. Fu R, et al. (2015) Clinical severity in Lesch-Nyhan disease: The role of residual enzyme and compensatory pathways. *Mol Genet Metab* 114:55–61.
21. Huang B, Wang W, Bates M, Zhuang X (2008) Three-dimensional super-resolution imaging by stochastic optical reconstruction microscopy. *Science* 319:810–813.
22. Kural C, et al. (2005) Kinesin and dynein move a peroxisome in vivo: A tug-of-war or coordinated movement? *Science* 308:1469–1472.
23. Encalada SE, Szpankowski L, Xia CH, Goldstein LSB (2011) Stable kinesin and dynein assemblies drive the axonal transport of mammalian prion protein vesicles. *Cell* 144: 551–565.
24. Maday S, Wallace KE, Holzbaur ELF (2012) Autophagosomes initiate distally and mature during transport toward the cell soma in primary neurons. *J Cell Biol* 196: 407–417.
25. Rook MS, Lu M, Kosik KS (2000) CaMKIIalpha 3′ untranslated region-directed mRNA translocation in living neurons: Visualization by GFP linkage. *J Neurosci* 20:6385–6393.